Reprinted from October 1991, Vol. 113, Journal of Tribology

The Measurement and Finite Element Analysis of the Dynamic Stiffness of Nonuniform Clearance, Gas, Thrust Bearings[1]

P. Holster

J. Jacobs

Philips Research Laboratories,
Eindhoven, The Netherlands

J. Roblee

Lawrence Livermore National Laboratory,
Livermore, Calif.

This paper presents an overview of a finite-element-method (FEM) approach for the calculation of the dynamic stiffness of circular, externally pressurized gas thrust bearings with a nonuniform clearance. Some observations are made about the characteristic behavior of gas bearings subject to dynamic loading. The primary emphasis of this paper, however, is the development and qualification of a test apparatus and the necessary test techniques for measuring dynamic stiffness up to 250 N/μm at frequencies up to 2000 Hz. A thorough, experimental verification of the FEM model is reserved for a later paper.

1 Introduction

Externally pressurized, circular, gas bearings are widely used as guides in slideways and as thrust bearings in spindles. Their main advantages are ease of manufacturing and large load per unit area. Unfortunately, gas bearing pads, particularly ones with nonuniform clearances, are sometimes prone to a pneumatic-hammer instability. In most gas-bearing designs, only the load, static stiffness, and flowrate of the gas bearings are considered. So long as the bearing is stable, the frequency dependence of its dynamic stiffness is seldom considered. Because externally-pressurized gas bearings exhibit damping only over a small frequency band, they are often reputed to be poorly damped. However, many applications of gas bearings would greatly benefit if their damping characteristics could be fully exploited.

To better utilize gas bearings, better computational tools were necessary to analyze and evaluate their dynamic behavior. The analytical results must also be verified experimentally. The primary purpose of this paper is to describe the test apparatus and test techniques we developed to measure the dynamic stiffness of gas, thrust bearings and to demonstrate the capabilities and limitations of the apparatus. Our goal was to develop a capability to measure dynamic stiffnesses up to 250 N/μm in magnitude with an accuracy better than 5 percent over a 0–2000 Hz frequency range.

2 Overview of the Dynamic Analysis of Gas Bearings by the Finite Element Method

The geometry of a nonuniform-clearance bearing of the type under consideration here is shown in Fig. 1. We propose to use the finite element method to analyze the dynamic stiffness of these bearings. In the FEM formulation, a special form of the one-dimensional, Reynolds equation for compressible flow through a circular, thrust bearing is used (Holster and Jacobs, 1987),

$$-\frac{1}{2\pi}\frac{\partial M}{\partial r} \equiv \frac{\partial}{\partial r}\left\{\frac{r\rho h^3}{12\eta}\frac{\partial p}{\partial r}\right\} = r\frac{\partial \rho h}{\partial t}.$$

This form of the Reynolds equation is expressed in terms of a mass flow balance. After rewritting this equation into the weak formulation and after partial integration, we can find for ideal gases ($p = \rho R_S T$) that

$$\int_{R_{in}}^{R_{out}} \left(\frac{\partial ph}{\partial t}\psi + \frac{ph^3}{12\eta}\frac{\partial p}{\partial r}\frac{\partial \psi}{\partial r}\right) r dr = \frac{-R_S T}{2\pi} M\psi \Big|_{R_{in}}^{R_{out}} = \frac{R_S T}{2\pi} M_{in} \qquad \forall\psi. \tag{1}$$

This equation must be fulfilled for all test functions ψ that are only prescribed at the boundaries. The boundary conditions used to evaluate the righthand side are,

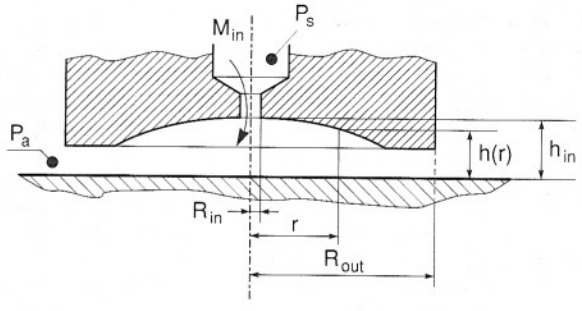

Fig. 1 Cross-sectional view of a bearing with a nonuniform clearance

[1]Work was performed at Philips Research Laboratories, and J. Roblee worked under the auspices of the U.S. Department of Energy by Lawrence Livermore National Laboratory under Contract No. W-7405-ENG-48.

Contributed by the Tribology Division of The American Society of Mechanical Engineers for presentation at the Joint ASME/STLE Tribology Conference, Toronto, Canada, October 7–10. Manuscript received by the Tribology Division March 26, 1990; revised manuscript received July 3, 1990. Paper No. 90-Trib-66. Associate Editor: J. A. Tichy.

Copies will be available until January 1992.

for $r=R_{in}$: $\psi=1$ and $M=M_{in}$,

and for $r=R_{out}$: $\psi=0$ and $p=p_a$.

Here M_{in} must equal the flow through the inlet restrictor which is modeled using a method described in Holster and Jacobs (1987). Equation (1) must be linearized in order to solve for the static pressure distribution $p(r) = p_0(r)$ with $h(r)=h_0(r)$. We found that a Newton iteration scheme can be conveniently employed to solve the resulting finite-element model. Due to the intricate nature of the inlet restrictor flow, we also needed to use a relaxation scheme to calculate the pressure recovery factor. From this computed pressure distribution, the static characteristics of load and gas flow can be determined for the bearing.

When we linearize equation (1) for the time dependent solution, we follow a similar procedure, but we use the static p_0 solution as a starting point. First we enforce a small, sinusoidal variation of the gap height with constant amplitude $\bar{h} \ll h_0$, this induces small in-phase, sinusoidal and out-of-phase, cosinusoidal, pressure variations. Therefore,

$$h=h_0+\bar{h}\sin\omega t$$

$$p=p_0+\bar{p}\sin\omega t+\bar{\bar{p}}\cos\omega t,$$

where the boundary condition at $r=R_{out}$ is $\bar{p}=\bar{\bar{p}}=0$. After substituting these into equation (1) and collecting the linear terms, the sinusoidal part is

$$\int_{R_{in}}^{R_{out}}\left(-h_0\omega\bar{\bar{p}}\psi+\frac{h_o^3}{12\eta}\left(\bar{p}\frac{\partial p_o}{\partial r}+p_0\frac{\partial\bar{p}}{\partial r}\right)\frac{\partial\psi}{\partial r}\right)rdr$$

$$-\frac{R_sT}{2\pi}\frac{\partial M_{in}^0}{\partial p_{in}^0}\bar{p}_{in}\Big|_{r=R_{in}}=$$

$$-\bar{h}\int_{R_{in}}^{R_{out}}\left(\frac{3p_oh_0^2}{12\eta}\frac{\partial p_o}{\partial r}\frac{\partial\psi}{\partial r}\right)rdr+\bar{h}\frac{R_sT}{2\pi}\frac{\partial M_{in}^0}{\partial h_{in}^0}\Big|_{r=R_{in}}\quad\forall\psi \qquad (2a)$$

and the cosinusoidal part is:

$$\int_{R_{in}}^{R_{out}}\left(h_0\omega\bar{p}\psi+\frac{h_0^3}{12\eta}\left(\bar{\bar{p}}\frac{\partial p_o}{\partial r}+p_0\frac{\partial\bar{\bar{p}}}{\partial r}\right)\frac{\partial\psi}{\partial r}\right)rdr$$

$$-\frac{R_ST}{2\pi}\frac{\partial M_{in}^0}{\partial p_{in}^0}\bar{\bar{p}}_{in}\Big|_{r=R_{in}}=-\bar{h}\int_{R_{in}}^{R_{out}}p_0\omega\psi rdr\quad\forall\psi \qquad (2b)$$

These two coupled equations must now be solved simultaneusly for the two unknown pressure distributions. Note that for $\omega=0$, equation (2b) gives $\bar{\bar{p}}=0$ and equation (2a) reduces to the static case for $\bar{p}$.

We can then apply Galerkin's method by approximating $\bar{p}$ and $\bar{\bar{p}}$ with the interpolation polynomials,

$$\bar{p}=\sum_{j=1}^{N}\bar{p}_j\,\phi_j \text{ and } \bar{\bar{p}}=\sum_{j=1}^{N}\bar{\bar{p}}_j\,\phi_j. \qquad (3)$$

To formulate the 1D FEM problem, the radius within the region $R_{in}<r<R_{out}$ is divided into $(N-1)$ line elements and one boundary element for the restrictor at $r=R_{in}$. In local coordinates, each line element has a length $\Delta=r_2-r_1$, and over that element the linear interpolation polynomials are $\phi_1=(r_2-r)/\Delta$ and $\phi_2=(r-r_1)/\Delta$. To derive the element equations, equation (3) is substituted into equation (2) and the integrals are evaluated over each element. By defining the following constants:

$$h_e=\frac{h_1+h_2}{2},\ r_e=\frac{r_1+r_2}{2},\ p_0^e=\frac{p_1^0+p_2^0}{2},\ \frac{\partial p_0^e}{\partial r}=\frac{p_2^0-p_1^0}{\Delta}$$

$$C_1=\frac{h_e^3r_e}{12\eta}\frac{1}{2}\frac{\partial p_0^e}{\partial r},\ C_2=\frac{h_e^3r_e}{12\eta}\frac{p_0^e}{\Delta},\ C_3=\frac{h_er_e\Delta}{3}$$

$$C_4=\frac{C_3}{2},\ C_5=\frac{3p_0^eh_e^2r_e}{12\eta}\frac{\partial p_0^e}{\partial r},\ C_6=\frac{p_0^er_e\Delta}{2}$$

the element matrix and the corresponding element vectors are related as

$$\begin{bmatrix}-C_1+C_2 & -\omega C_3 & -C_1-C_2 & -\omega C_4\\ \omega C_3 & -C_1+C_2 & \omega C_4 & -C_1-C_2\\ C_1-C_2 & -\omega C_4 & C_1+C_2 & -\omega C_3\\ \omega C_4 & C_1-C_2 & \omega C_3 & C_1+C_2\end{bmatrix}\begin{Bmatrix}\bar{p}_1\\ \bar{\bar{p}}_1\\ \bar{p}_2\\ \bar{\bar{p}}_2\end{Bmatrix}\leftrightarrow$$

$$-\bar{h}\begin{Bmatrix}-C_5\\ \omega C_6\\ C_5\\ \omega C_6\end{Bmatrix}$$

and the boundary element at $r=R_{in}$ is

$$-\frac{R_sT}{2\pi}\frac{\partial M_{in}^0}{\partial p_{in}^0}\begin{bmatrix}1 & 0\\ 0 & 1\end{bmatrix}\begin{Bmatrix}\bar{p}\\ \bar{\bar{p}}\end{Bmatrix}\leftrightarrow\bar{h}\frac{R_sT}{2\pi}\frac{\partial M_{in}^0}{\partial h_{in}^0}\begin{Bmatrix}1\\ 0\end{Bmatrix}. \qquad (5)$$

Here the $\leftrightarrow$ symbol is used because an equal sign can only be rigorously applied to the global matrix obtained from the assembly of these element matrices. At a particular frequency, the solution for $\bar{p}_j$ and $\bar{\bar{p}}_j$ are straightforwardly determined by means of a standard, finite-element, computer code. The code assembles the global matrix of dimension $2(N-1)\times 2(N-1)$, which is then solved to obtain the $2(N-1)$ unknown pressures. Note that the solutions for the nodal pressures are linearly dependent upon $\bar{h}$, the amplitude of the height variation. Finally, the in-phase pressure, $\bar{p}$, and the out-of-phase pressure, $\bar{\bar{p}}$ can be integrated to obtain the real and imaginary parts of the dynamic stiffness of the bearing at the frequency ω,

$$K=\bar{k}+i\,\bar{\bar{k}} \text{ where } \bar{k}=\frac{2\pi}{\bar{h}}\int_{R_{in}}^{R_{out}}\bar{p}rdr \text{ and}$$

$$\bar{\bar{k}}=\frac{2\pi}{\bar{h}}\int_{R_{in}}^{R_{out}}\bar{\bar{p}}r\,dr.$$

Nomenclature

a = acceleration, m/s^2
F = force, N
h = gap height, m
$\bar{h}$ = amplitude of gap-height variation, m
k, K = stiffness, N/m
M = mass flow, kg/s
N = number of nodes on a radial line
p = pressures, Pa
$\bar{p}, \bar{\bar{p}}$ = in-phase and out-of-phase components of dynamic pressure, Pa
p_a, p_s = ambient and supply pressure, Pa
$\bar{p}_j$ = solution vector of nodal pressures, Pa
r = polar coordinate in the radial direction, m
R_s = specific gas constant, J/kg-°K
s = Laplace variable, s^{-1}
t = time, s
T = temperature, °K
Δ = length of a line element, m
η = absolute viscosity, N-s/m^2
ρ = density, kg/m^3
τ = time constant, s
ϕ = interpolation polynomials
ψ = test functions
ω = angular velocity, rad/s

Indices

b = a bearing property
o = static condition
in = at the inner radius
k = Kistler force transducer
out = at the outer radius
e = an element property

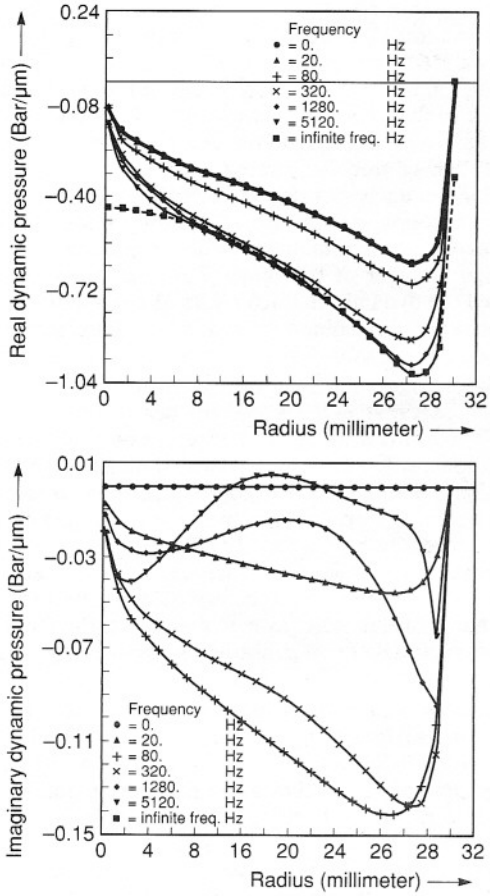

Fig. 2 Example solution of the dynamic pressure distributions in a 60 mm diameter bearing, with a 13 μm conicity and a 0.53 mm diameter feed hole: Operating conditions: supply pressure = 6 baro, minimum clearance = 3 μm, load = 1189 N.

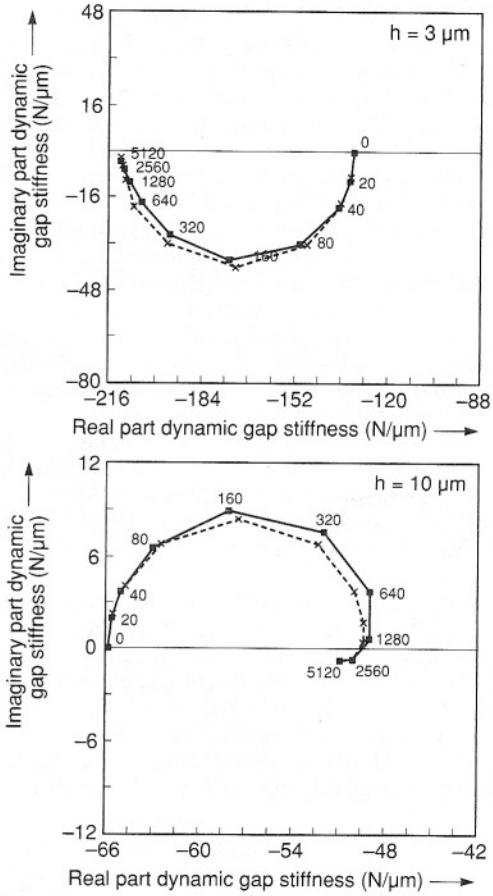

Fig. 3 Calculated dynamic stiffnesses plotted on a Nyquist diagram for a minimum clearance of 3 and 10 μm. The numbers on the plots indicate frequencies in Hertz. The dashed line is a second order model correlated to the calculated data.

3 Characteristic Behavior of Gas Bearing Dynamics

The dynamic-pressure distributions shown in Fig. 2 illustrate typical solutions of equation (2) for a conically shaped air bearing at different frequencies of gap oscillations. Note how the pressure distributions smoothly evolve as the frequency increases. At high frequency, the pressure distributions converge to the trapped-gas pressure distribution which has a zero imaginary part. This infinite-frequency solution is easily calculated by using Boyle's Law (Langlois, 1962), and knowledge of the static pressure distribution and gas-film thickness. Not only does Boyle's Law provide an independent check of the time-dependent, finite-element solution, but it can provide an indication of bearing stability. When the real, dynamic pressure at high frequency exceeds the static change in pressure for $\bar{h}$, the bearing will generally be stable (Roblee and Mote, 1985 and 1986a).

After integrating the pressure distributions of Fig. 2, the resulting dynamic stiffness is plotted on a Nyquist diagram in Fig. 3(*a*). In this diagram, a negative imaginary part corresponds to a positive damping characteristic in the bearing, which means the bearing will dissipate the kinetic energy of an oscillating bearing at those frequencies. The Nyquist plot in Fig. 3(*a*) corresponds to a minimum bearing-clearance of 3 μm. Under this condition, the bearing has positive damping at all frequencies. However, when the minimum clearance is increased to 10 μm by a decrease in the applied load, as in Fig. 3(*b*), the bearing demonstrates a negative damping characteristic for frequencies below 1500 Hz. Consequently this bearing would be unstable if there were enough mass riding on it (>0.56 kg) so that the mass-bearing natural frequency is below 1500 Hz.

The mostly semi-circular shapes of the Nyquist plots in Fig. 3 indicate that the frequency responses are similar to those of the pole-and-zero transfer function (Takahashi et al., 1970)

$$K_b(s) = K_0 \frac{1+\tau_1 s}{1+\tau_2 s}$$

In the case of Fig. 3(*b*), where two semi-circles are evident, the response correlates to two, pole/zero pairs. To demonstrate this point, a two-pole, two-zero transfer function was fitted to the calculated frequency responses in Fig. 3. The result is illustrated by the dashed lines on the charts. This type of pole/zero behavior is characteristic of many types of gas bearings, as illustrated by past test data (Plessers and Snoeys, 1988; Roblee and Mote, 1985, and 1986a) and other dynamic models (Lohiya and Pande, 1989; Roblee and Mote, 1985, 1986a, 1986b; and Langlois, 1962).

The fact that gas bearings have this pole/zero-type behavior has important implications for the test apparatus and techniques needed to measure their dynamic stiffness. Because their dynamic stiffness is a smooth function of frequency, with real-valued asymptotes at low and high frequency, a bearing's dynamic response does not need to be characterized over a wide frequency spectrum. Unlike a mechanical structure, a gas-bearing's dynamic stiffness will not have many large, sharp peaks or drop to near zero over narrow frequency bands. Consequently, if such phenomena are observed in the measurements, they must be an artifact of the test apparatus itself. This intrinsic behavior of gas bearings allows them to be characterized by data from only selected portions of the frequency spectrum.

4 Description of the Test Apparatus

In principle the measurement of dynamic stiffness of a gas bearing is the same as for any other object. Namely, a known, time-varying load must be applied, and the resulting deformation must be measured. Standard tensile-test machines have this capability for slowly varying loads. However, a number of complications arise when a gas bearing is to be characterized. First, a gas bearing must be preloaded with a large, static load in order to establish its nominal gap height at a given supply pressure. Then a small dynamic load must be superimposed on the static one so that the gap-height variation is less than 1 percent of the total gap height. For any larger load, the response of the bearing would become more and more nonlinear as the amplitude increases, which is not of interest for most applications of gas bearings (see Section 2 also). Accurate measurement of nonlinear stiffness over a wide frequency range is also much more difficult to achieve. Because the nominal gap height may only be 3 μm, a very high resolution, motion sensor must be used. Care must also be taken so that the structural loop between the motion sensor and bearing surfaces does not introduce measurement errors in the 0–2 kHz frequency band.

To develop this dynamic-stiffness-measuring capability we choose to modify an existing apparatus that had been used to measure the static properties of gas bearings (Holster and Jacobs, 1987), such as load, gap height and flow. The result of this effort is shown in Fig. 4, where an overview of the entire test apparatus is presented, and Table 1 lists the instrumentation used to perform the measurements. Starting from the bottom, the parts of the apparatus are described in the following.

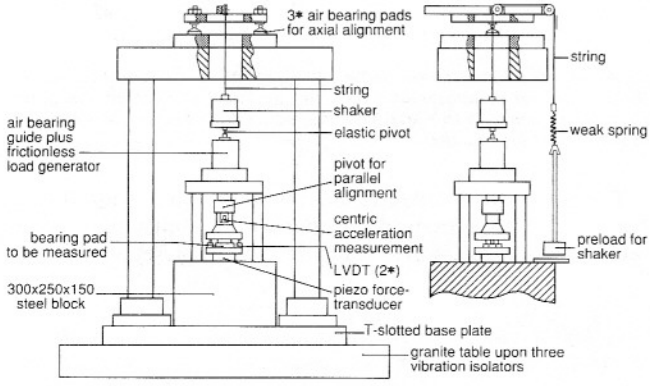

Fig. 4 Illustration of the test apparatus

A granite base (900*700*70 mm^3) is mounted on three vibration isolators. Thereupon rests a standard, T-slotted, base plate (1000*640*40 mm^3) on which a 90 kg steel block (300*250*150 mm^3) is mounted. Beneath the steel block is a 1 mm thick rubber sheet. The basic principle of this design is to have a base with a large inertia and well damped resonances in the 0–2 kHz frequency range of the measurements. The measuring set-up is positioned centrally with respect to the base so that coupling to the natural bending modes of vibration of the base plate is minimized. This base design is the final result of a number of trial configurations that progressively improved the dynamic characteristics of the apparatus. Measurements of the dynamic response of the base are presented in Section 5.

A Kistler, piezo-electric, force transducer is mounted between the heavy, steel block and the bearing pad to be measured. The force transducer is prestressed by 5000 N to obtain a high contact stiffness. The use of the standard washer proved to be essential for obtaining good force data, otherwise the force transducer's output was sensitive to the bending of its upper surface. On both sides of the bearing pad, two LVDT-type, displacement transducers are mounted so that they can directly measure the gap-height variation of the bearing. We found that for frequencies as high as 400 Hz, the LVDTs have sufficient accuracy if compensation is used for the amplifier's frequency response.

The bearing pad is opposed by a surface that is flat within 0.1μm. This surface is rigidly supported so that the bearing gap will not be influenced by it bending under the applied load. The opposing piece attaches to an air-bearing-guided ram by means of a pivot joint which allows the loading surface to align itself to the bearing. The ball pivot also insures that the applied force is transmitted through the centerline of the loading surface, without inducing any moment loads. An accelerometer can also be mounted on the centerline of the loading piece, where it will be insensitive to its tilting motions. The large, static, bearing load is generated in a chamber above the ram, where pressurized air acts upon a piston. The chamber pressure is controlled by an ultrastable, precision regulator, and loads up to 1500 N can be generated. This device is described in more detail in Holster and Jacobs (1987).

On top of the loading device, a voice-coil-type minishaker is mounted to an elastic pivot. The shaker is counterweighted by a string which is guided over two rollers on a pedestal. The rollers can be floated on three air-bearing pads so that the string can be aligned with the ram. The soft spring on the string dynamically decouples the counterweight from the

Table 1 List of instrumentation

Device	Make and model	Sensitivity/range	Resolution	Output levels
Structural Dynamics Analyzer	Hewlett-Packard 5423A	70 db dynamic range, 0–20 kHz	1μV 400 frequency lines	±10V random noise
Power Amplifier	Bruel and Kjaer 2706	10 Hz to 20 kHz		75 W with attenuator
Mini-shaker	Bruel and Kjaer 4810	± 7N force 20 Hz-18 k-Hz		±3 mm stroke, 15 W power
Accelerometer	Bruel and Kjaer 4371	0.984 pC/m-s^{-2} 0.2–9100 Hz		
Force Transducer	Kistler 9061	4.01 pC/N 0–200,000 N, 0–45 kHz	<0.01 N	
Charge Amplifier	Bruel and Kjaer 2635	w/4371: 1.0 m/s^{-2} w/9061: 0.1V/N 2 Hz–100 kHz	5×10^{-3}pC (2Hz to 22kHz)	Integrates acceleration, ±8V
Charge amplifier	Kistler 5001	w/9061 0.01V/N 0–180 kHz	2×10^{-3} pC rms	Up to 100,000 sec time constant, ±10V
LVDT displacement transducer	TESA probes: GT42 power supply: 302 amplifier: 401	0.324 V/μm 0–160 Hz (−3 db)	<0.06 μm	±1.0V

Table 2 Summary of the important mechanical parameters of the test apparatus

$m_5 = 1.04$ kg	The mass of the counterbalance hanging on the string connected to the minishaker.
$k_5 = 10^3$ N/m	The stiffness of the soft spring on the string
$m_4 = 1.0$ kg	The mass of the minishaker housing.
$k_4 = 2*10^3$ N/m	The stiffness of the flexures inside the minishaker.
$m_3 = 0.875$ kg	The mass of the entire piston and ram assembly, including the opposing bearing surface and the minishaker core.
$k_3 = 10$ to $250*10^6$ N/m	The stiffness of the bearing film.
$m_2 = 1.4$ kg	The mass of the bearing pad plus mounting plate.
$k_2 = 4*10^9$ N/m	The measured stiffness of the Kistler force transducer, including its contact stiffness.
$m_1 = 400$ kg	The mass of the granite table, T-slotted plate, the steel block plus everything fixed upon it.
$k_1 = 10^6$ N/m	The stiffness of the vibration isolators underneath the granite table.

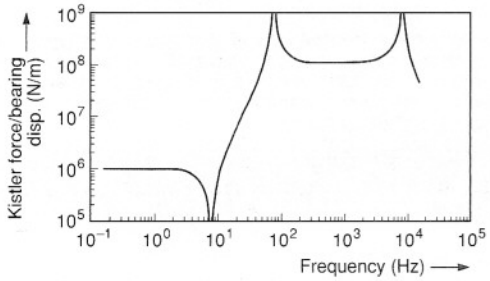

Fig. 5 An analytical model of the experimental apparatus with a bearing of a constant 10^8 N/m stiffness. This amplitude portion of a Bode plot illustrates the response of the force transducer to the absolute displacement of the loading ram.

shaker is then able to generate the dynamic forces necessary to perform the desired measurements.

5 Qualification Tests of the Apparatus

The configuration of the test apparatus presented above, including the type and location of the transducers, was chosen carefully. Special consideration was given to the dynamic interaction of the structural apparatus, transducers and their mounts, and the gas bearing itself. Each transducer also has its own limitations, but even with ideal transducers, the interaction with the apparatus can limit out ability to measure the bearing's dynamic-stiffness. To better understand how the apparatus can influence the frequency range and accuracy of our measurements, we constructed a simplified, lumped-mass/spring model of its major components. Table 2 lists the values of the five masses and five springs that comprise the model, along with a description of the component it represents. As is apparent from the topology of the apparatus, the springs interconnect the masses in a series fashion, with k_1 connecting m_1 to ground and on through k_5 connecting m_5 to the top of m_4.

In this model the force generated by the coil of the shaker acts across spring k_4, while the compression of spring k_2 prescribes the output of the Kistler force transducer shown in Fig. 4. The previously mentioned accelerometer measures the absolute acceleration of the ram, m_3, whereas the LVDTs measure the displacement of m_3 relative to m_2. Unfortunately the behavior of the LVDTs limit their use to frequencies below 400 Hz. Conversely, high-sensitivity accelerometers have an unrivaled ability to detect minute motions at high frequencies.

Because accelerometers measure absolute motion, the ideal measurement situation would have the bearing mount be fixed

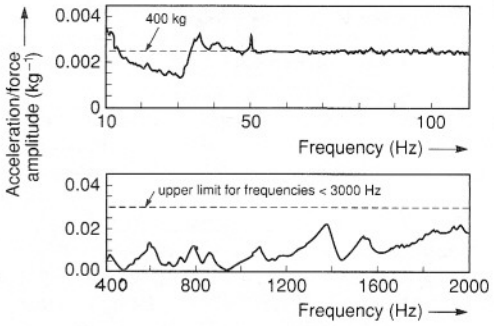

Fig. 6 Dynamic response of the gas bearing mount within the experimental apparatus. This amplitude portion of a Bode plot relates mount acceleration to force measured on its upper part.

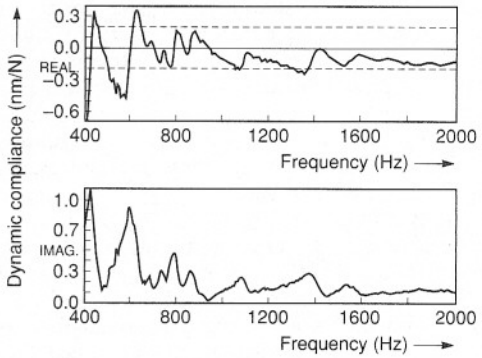

Fig. 7 Absolute displacement response of the bearing mount to an applied force measured by the force transducer

relative to the inertial frame of the Earth. Then the bearing's dynamic-stiffness could be determined by measuring only the acceleration of the opposing surface when a known, dynamic load is applied. In practice, however, this ideal situation can only be approximated by fixing the bearing pad to a base with a large mass. If the base is massive and rigid enough, the acceleration of the bearing pad will be negligible (< 1 percent) compared to that of the opposing surface. To test this hypothesis a bearing stiffness of 100 N/μm was used in the lumped-mass model, and the transfer function of the absolute displacement (integrated acceleration) of m_3 and the compression of k_2 was calculated using MATLAB. The amplitude part of this transfer function is plotted in Fig. 5. The stiffness of the isolators is evident at frequencies below 2 Hz, but only between 300 and 2000 Hz does the response closely match the 100 N/μm stiffness of the bearing. The resonance at 7.9 Hz is a result of the entire apparatus moving on the isolators, whereas the stiffness peak at 79 Hz is a result of an anti-resonance of the table mass, m_1, on the bearing film. The frequency of this peak would shift to 126 Hz if the bearing stiffness were 250 N/μm. The last stiffness peak, at 8600 Hz in Fig. 5, is a result of the bearing mount, m_2, resonating on the force transducer, k_2. The three other vibration modes of the test apparatus do not affect the transfer function plotted in Fig. 5. Those modes are at 3.8 Hz for m_5 on k_5, at 9.3 Hz for m_4 on k_4, and at 1700 Hz for m_3 on the bearing film, k_3. The insensitivity to the 1700 Hz mode is a direct result of locating the force transducer below the bearing, as opposed to attaching it to the ram. We conclude from this analysis that an LVDT measurement of gap-height variation to 400 Hz is more than sufficient to cover the low-frequency band where a single accelerometer measurement produces inaccurate stiffness estimates. To qualify the measuring setup, we mounted a force transducer at the position where the bearing normally mounts. Onto the force transducer, a mini-shaker was attached via an elastic pivot.

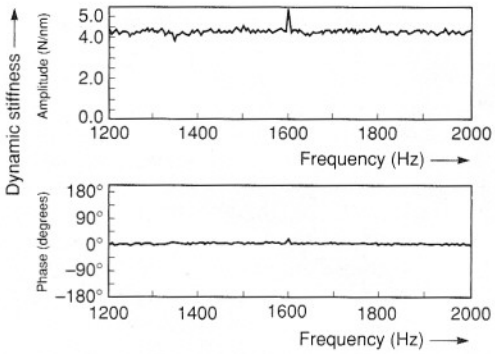

Fig. 8 Dynamic stiffness of the Kistler force transducer and its mounting hardware as determined from relative acceleration measurements

Figure 6 shows the amplitudes of a transfer function measured between an accelerometer mounted on the top side of the bearing mount and the output of the force transducer. If the table were perfectly rigid this a/F response should correspond to the inverse of the table mass, 0.0025 kg^{-1}, as it does in Fig. 6(a). Figure 6(b) however, shows a number of unmodelled resonances of the table. Note that these resonances are well damped, which is a result of several, careful redesigns of the apparatus. When the data of Fig. 6(b) is integrated twice, the dynamic compliance of the bearing mount is obtained. The real and imaginary parts of this dynamic compliance are shown in Fig. 7. If this motion were neglected, as in a single accelerometer measurement of a bearing's dynamic-stiffness, the error in the real part of the measurement will exceed 5 percent at only a few frequencies when the bearing has a compliance of 4nm/N. However, the imaginary (out-of-phase) part of the dynamic compliance is usually much smaller than the real part for most gas bearings. Consequently, the percent error for the imaginary part will be much larger.

The bearing-mount acceleration shown in Fig. 6 introduces one other error to the measurement of bearing dynamic-stiffness. Because the force transducer is separated from the bearing surface by an object with mass, $m_2 = 1.4$ kg, its acceleration causes the measured force F_k to differ from the force F_b acting on the gas film of the bearing. Applying Newton's Law to m_2 illustrates the error,

$$F_b/F_k = 1 + m_2\, a/F_k. \tag{6}$$

The a/F_k data from Fig. 6 indicates that this mass effect increases the measured stiffness by less than 5 percent at frequencies up to 3 kHz. When the mount acceleration is measured, however, equation (6) can be applied to compensate for this error. This mass effect was also present in the idealized model of the test apparatus. In this case, however, the table is considered, so then $m_2 a/F_k$ is less then 0.01 below 1000 Hz and therefore it has an insignificant effect on the transfer function of Fig. 5.

The motion of the bearing mount can be compensated for by taking two accelerometer measurements, one on each side of the bearing. The average of these two, a/F transfer-function measurements gives the motion of the mount at its centerline, which can then be subtracted from the ram accelerometer data. If different accelerometers are used for these measurements, their frequency response must be closely matched or else other errors will be introduced. By this technique, bearings with much higher stiffness than 250 N/μm can be measured accurately. This fact is illustrated by the dynamic-stiffness measurement of the Kistler force transducer shown in Fig. 8. Here four accelerometer measurements were used, two on top of the force transducer and one on each side. The flatness of the stiffness amplitude and the near zero phase demonstrate how well the mount-plus-table motion of Fig. 7 can be compensated for. The well-damped frequency response of the table aids this process because very accurate transfer-function measurements can be made with the limited dynamic range and frequency resolution of the spectrum analyzer (Otnes and Enochson, 1978).

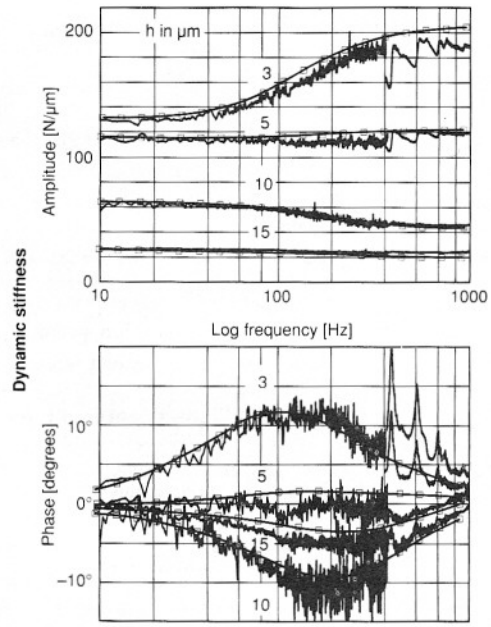

Fig. 9 Calculated and measured dynamic stiffness of the 13 μm conical bearing at minimum clearances at 3, 5, 10, and 15 μm and with a constant supply pressure of 6 baro. LVDT data are used up to 400 Hz and a single accelerometer measurement is used from 400 to 1200 Hz.

6 Prototype Bearing Measurement

In this section we describe the procedures used to measure the dynamic stiffness of a prototype bearing. This bearing is circular, with an outer diameter of 60 mm, an inlet hole of 0.53 mm and a conicity of 13 μm, which match the bearing analyzed in Figs. 2 and 3. This particular bearing is prone to pneumatic hammer at supply pressures larger than 6 bar gauge pressure, which makes it an interesting one to examine.

The static measurements of load and flow showed a good agreement with the computer model when the measured gap height is corrected by $+0.5$ μm. A $+0.5$ μm discrepancy in the gap measurement is typical considering the errors involved in establishing a zero-gap reference for the LVDTs. The close agreement with the static solution is encouraging because it is the starting point for the dynamic-stiffness calculations. For a supply pressure of 6 bar, the calculated values of dynamic stiffness are shown in the amplitude and phase diagrams of Fig. 9 for four different gap-heights. The 3 and the 10 μm solutions are the same as the ones shown in the Nyquist diagram of Fig. 3, but here only the frequency range of 10 to 1200 Hz is presented.

For the same four gap-heights used in Fig. 9, the dynamic stiffnesses were measured on the test bearing. The dynamic measurements were performed over three frequency bands, using a band-limited excitation force:

10 - 110 Hz: displacements measured with LVDT probes
50 - 450 Hz: displacements measured with LVDT probes
400 - 1200 Hz: ram acceleration measured only.

The three sets of dynamic stiffness data for each gap-height are plotted with the computed stiffnesses in Fig. 9. The agreement is good, especially considering the 0.5 μm discrepancy in the gap-height measurements. The pole/zero-type frequency response of the bearing is very apparent in the measurements. The good agreement where the data sets overlap, in the 50–110 Hz and the 400–450 Hz bands, demonstrates the consist-

ency of the test apparatus and the measurement techniques. The largest discrepancy between data sets occurs in the phase measurement by the LVDTs and the accelerometer near 400 Hz. The 4° discrepancy is a residual error in the compensation of the frequency response of the LVDT amplifier. This error is reduced to an undetectable level at frequencies below 150 Hz.

One indicator of measurement quality is the smoothness of the plots in Fig. 9, which are the averages of 40 measurements each. The measurement quality degrades when the dynamic stiffness of the bearing under test is large. This degradation is primarily due to the resolution limits of the motion sensors in detecting the small displacements (< 10 nm rms) or small accelerations of a stiff bearing being excited by a limited force. The resolution limits of the LVDTs are also evident when the 10–110 Hz data sets are compared to the 50–450 Hz data sets. The wide frequency-band measurement is noiser because the excitation force is more widely distributed, which lowers the signal-to-noise ratio of the LVDT at any given frequency. The coherence (Otnes and Enochson, 1978), of the LVDT and the force transducer signals also indicates a loss of data quality with a stiff bearing, as it drops from near 1.0 at low frequency to less than 0.95 at 450 Hz. This problem could be reduced by taking more LVDT measurements over narrower frequency bands, but this will be at the expense of increased testing time. Figure 9 shows the lower noise data that are obtained from the accelerometer at 400 Hz as compared to the LVDT data. This is due to the acceleration level increasing with the square of the frequency, while the displacement spectra is nearly flat in this frequency band. Also, the LVDT amplifier attenuates the signal as much as 8 dB at 400 Hz. Below 200 Hz, the accelerometer signal is much noisier than the LVDTs, which was evidenced by other coherence measurements. The good coherence as well as the consistent data, even at reduced excitation levels, indicate that the dynamic response of the bearing is predominantly linear for the small (< 2N rms) exicitation forces used here, which satisfies one of our measurement objectives.

The data presented in Fig. 9 are a result of an expedient measurement procedure where the bearing can be quickly characterized. The penalties of this procedure are apparent when the dynamic stiffness is high. Not only is the LVDT data noiser, but the undulations in the accelerometer data, particularly between 400 and 800 Hz, are larger. These undulations in dynamic stiffness are not due to the behavior of the gas film, but they are a result of the motion of the bearing mount on the table (see Fig. 7). The table motion could be subtracted out if two more accelerometer measurements are made. With this more time consuming procedure, much stiffer bearings could be tested to frequencies approaching 3 kHz. However, the quality and quantity of the data in Fig. 9 is still more than adequate to identify the dominant, pole/zero response of this particular bearing, even if the data between 400 and 800 Hz is ignored.

7 Conclusions

We have developed a finite-element, computer code to model the dynamic stiffness of externally pressurized gas, thrust bearings. In particular, we were able to incorporate an accurate model of the restrictor flow in the code. Our initial results are consistent with past observations and other models, but the code has yet to be completely verified with experimental results. A future paper will provide more details about the code, our experiences with its use, and a thorough experimental-verification study.

The primary outcome of our current work is the development of a general-purpose apparatus for measuring the static and dynamic stiffnesses of small objects ($< 60 \times 60 \times 60\ mm^3$) under static loads of up to 1500 N. With this apparatus, we have developed techniques for measuring dynamic stiffnesses greater than 250 N/μm and over a frequency range of 10 to more than 2000 Hz. The measured dynamic-stiffness amplitudes are accurate to better than 5 percent while using excitiation forces of only 2N rms. The test apparatus and techniques provide consistent, reliable data that can be efficiently obtained. With this test apparatus and test techniques, the dynamic stiffness of a prototype, gas bearing was measured. We were able to successfully characterize the bearing's dominant, pole/zero-type frequency response in the frequency range where it is normally utilized (10–1200 Hz). The measurement results show the frequencies where the bearing has the most damping and where it could go unstable. As a result of this work, we now have a fully qualified, dynamic-stiffness-measurement capability. We anticipate that this capability will allow us to understand the dynamic response of gas bearings more fully than before, which will permit their use in more demanding applications.

References

Holster, P., and Jacobs, J., 1987, "Theoretical Analysis and Experimental Verification of the Static Properties of Externally Pressurized Air-bearing Pads," *Tribology International*, Vol. 20, No. 5, pp. 276–289.

Huebner, K. H., 1975, *The Finite Element Method for Engineers*, Wiley, New York, NY.

Lohiya, S. H., and Pande, S. S., 1989, "Analysis of Tapered Land Aerostatic Thrust Bearings Operating Under Non-Steady Loads," *Mech. Mach. Theory*, Vol. 24, No. 6, pp. 515–521.

Langlois, W., 1962, "Isothermal Squeeze Film," *Quarterly of Applied Mathematics*, Vol. XX, No. 2, pp. 131–150.

Otnes, R,. and Enochson, L., 1978, *Applied Time Series Analysis*, Vol. 1, *Basic Techniques*, Wiley, New York, NY.

Plessers, P., and Snoeys, R., 1988, "Dynamic Identification of Convergent Externally Pressurized Gas-bearing Gaps," ASME JOURNAL OF TRIBOLOGY, Vol. 110, pp. 263–270.

Roblee, J., and Mote, Jr., C., 1986a, "Vibration Damping in Externally Pressurized Gas Bearings," Lawrence Livermore National Laboratory; Livermore, California; UCRL-93600 Preprint, Presented at the International Conference of Vibration Problems in Engineering, Xi'an, China.

Roblee, J., 1986b, "Design of Externally Pressurized Gas Bearings for Stiffness and Damping," Lawrence Livermore National Laboratory, Livermore, Califnorina, UCRL-95314 Preprint, Presented at the 9th International Gas Bearing Symposium, National Bureau of Standards, Washington, DC.

Roblee, J., 1985, "Design of Externally Pressurized Gas Bearings for Dynamic Applications," Ph.D. thesis, University of California; Berkeley, Calif.

Takahashi, Y., Rabins, M., and Auslander, D., 1970, *Control and Dynamic Systems*, Addison-Wesley, New York, NY.

DISCUSSION

F. Al-Bender[2]

The authors make an interesting contribution to the problem of evaluating the dynamic characteristics of aerostatic bearings. With special emphasis laid on experimental verification, they give a detailed description of the test setup and an elaborate discussion of its capabilities and limitations. Their work falls short, however, of establishing a design methodology for such an apparatus. This seems to be due to (*a*) aiming at a general purpose apparatus not restricted to evaluating air bearings alone; and (*b*) starting from a given structure, originally designed for static tests, and trying to modify it to accommodate dynamic testing. The results they obtain thus do not constitute a significant advance upon those obtained by Plessers (1988) who used essentially the same type of test apparatus.

[2]Katholieke Universiteit Leuven, Department of Mechanical Engineering, Leuven, Belgium.

With regard to point (*a*) above, an essential distinction may be made between a "black box" and a component whose characteristic equations are known in that the latter yields to dimensional analysis whereas the former can only be dealt with using absolute quantities which may be very misleading both with respect to general characterization as well as error estimation of observation. Normalization, on the other hand, leads to similitude criteria which facilitates appropriate scaling both of test object and apparatus. If we, thus, normalize this particular problem (see e.g., Gross (1962)) we may distinguish the following dimensionless (design) parameters:

$$\bar{R} = R_{in}/R_{out},\ \bar{h}_v = h_{in}/h_{out},\ \bar{p}_s = P_s/P_a,$$

$$\Lambda = \frac{24 C_d \mu \sqrt{(R_s T_s)} \cdot R_{out}}{P_a \cdot h^2_{out}} \quad \text{(the feed number)},$$

$$\sigma = \frac{12 \mu \omega}{P_a} \left(\frac{R_{out}}{h_{out}}\right)^2 \quad \text{(the squeeze number)},$$

(where C_d is the coefficient of discharge of the in-flow, and μ is the viscosity of the fluid).
This set of parameters determines the dimensionless bearing characteristics:

$$\bar{F} = \frac{F}{\pi R^2_{out} \cdot P_a} \qquad \bar{K}(\sigma) = K(\omega) \cdot \frac{h_{out}}{\pi R^2_{out} \cdot P_a}$$

(dimensionless Force) (dimensionless stiffness)

We note especially that the dimensionless stiffness (which is complex valued) appears as a function of the squeeze no. σ (rather than the frequency,) a circumstance which allows scaling (up or down) of the test frequency domain by one or a combination of the remaining absolute parameters in σ, in particular the bearing geometry (R_{out}/h_{out}). Such a starting point (viz. based on normalized equations) would, in our opinion, provide for a more systematic treatment of the problem.

A few other points about the theory will not be out of order here. Firstly the proposed use of the FEM to solve a linearized differential equation seems, in our view, superfluous since such an equation may be solved more accurately, simply and efficiently by conventional techniques (e.g., Euler's method through to Runge-Kutta). It would be interesting indeed if the unlinearized eq. 1 were to be solved by FEM, so as to compare the results with those obtained by Plessers (1988) using a predictor-corrector scheme. It was, further, shown by this solution that linearization would be valid if the excitation amplitude were to remain within about 5 percent of the nominal static value of the film thickness (such will give a better measurement possibility than the 1 percent value used by the authors). Moreover, it may be interesting to gauge the influence of the amplitude on the dynamic behavior.

The authors are to be commended for taking particular care of the restrictor flow model. The passive stiffness (Blondeel et al., (1980)) of the gas film has always positive damping; the gap transfer function always negative: the restrictor transfer function determines the net effect. However, most restrictor flow formulas, including the one used by the authors, fail to characterize adequately the complex flow phenomenon around the feed-hole lumping the problem, in space, at one point and excluding time dependence. This should be recognized as an important source of error in the theoretical model (i.e. that the quasi-static treatment of the restriction flow is only a first approximation).

As for point (*b*), viz. by starting from a given structure and trying to "tune" it, one is likely to run into a series of increasing complications (as is presented in Sec. 5 of the paper). In theory, if the total system were both damped and deterministic, then it would be possible to extract the dynamic characteristics of its various component parts, in particular that of the test object. In practice, however, such conditions cannot always be insured, especially over a broad frequency range, and the need to simplify the system always arises. The attempt to compensate for the various sources of error, in a complex system, e.g. by accelerometers... etc., cannot provide a satisfactory solution since such compensation inevitably introduces its own errors and we may end up by increasing uncertainty rather than reducing it; the answer lies rather in removing or strongly attenuating the very source of error by adoption of a clear and simple design methodology. Central in such a design, stand the bearing components and their immediate vicinity that should be better optimized with respect to mass and geometry. An excellent treatment of the stability of mechanical structures containing aerostatic bearings is given in Plessers and Snoeys (1980) that may prove useful in designing an efficient test apparatus.

Some remarks about the test apparatus and instrumentation might not be out of place. First, it is not clear why the authors treat the system as an axial series of masses and springs (Section 5 and Table 2) whereas Fig. 4 shows that the bearing is connected in parallel with the structure (a series configuration would be possible only if the bearing were made to support a free mass load). Furthermore, such an arrangement tends to make the model 3 dimensional with the possible appearance of vibration modes, other than the axial ones, but coupled with them, making the system even more complex than what is presented in Fig. 5. Bearing preload may also pay a role here (from our experience), and an experimental verification of the results of Fig. 5 becomes indispensable, (rather than verifying the system through the test object itself).

Second, the geometrical accuracy of the system is not discussed while there seems to be no means of ascertaining parallelism of the air gap: two displacement sensors are clearly not sufficient to establish parallelism. Centrally fed aerostatic bearings (as our research shows,) have very small tilt stiffness which decreases (as may intuitively be inferred,) with increasing dimensionless conicity $\bar{h}_v$. Tilt is encouraged by the location of the pivot point high above the bearing surface, which in turn seems to be dictated by the necessity to include an accelerometer in between. Nor is it clear why LVDT's, with their possible "contact" phenomena, are preferred to contactless sensors.

Last, nothing is mentioned about the repeatability of the results displayed in Fig. 9 whose reliability is greatly impaired by their noisy character. The agreement with the theory, as is also the case with that of Plessers and Snoeys (1988), may be taken only with reservation, especially the damping values which are of primary interest. The test apparatus is, in our opinion, still needy of further modification/qualification, if not a redesign, in light of this discussion.

Additional References

1 Plessers P., and Snoeys, R., 1988, "Dynamic Identification of Convergent Externally Pressurized Gas-Bearing Gaps," ASME JOURNAL OF TRIBOLOGY, Vol. 110, Apr., pp. 263-270.

2 Plessers, P., and Snoeys, R., 1988, "Dynamic Stability of Mechanical Structures Containing Externally Pressurized Gas-Lubricated Thrust Bearings," ASME JOURNAL OF TRIBOLOGY, Vol. 110, pp. 271-278.

3 Blondeel, E., Snoeys, R., and Devrieze, L., 1980, "Dynamic Stability of Externally Pressurized Gas Bearings," ASME JOURNAL OF LUBRICATION TECHNOLOGY, Vol. 102, Oct. pp. 511-519.

4 Gross, W. A., 1962, *Gas Film Lubrication*, Wiley.

Authors' Closure

Philips Research has had good contacts with Leuven University in the past (Prof. Snoeys and his graduates Dr. Blondeel, Dr. Devrieze, and Dr. Plessers). Now the comments of the discusser seem to be based on his lack of appreciation of

our work, that only perfects their work. We hope that the following answers will change his mind.

1. Although we did not attempt to give a design methodology for the test apparatus the following two simple startingpoints were used. First we tried to measure load and gap change of the bearing as close to the bearing as possible. Second, we designed for a one-dimensional case by assuring the load to be transmitted through the centerline. The combination of static and dynamic measurements into one apparatus is a big advantage because we assure equal settings. We claim a significant improvement on Plesser's apparatus because ours is simpler, easier to operate and goes up to higher frequencies for objects with even higher stiffness. We did not aim to design a general purpose apparatus but it came out to be one, and it is a cost effective design.

2. The question about dimensionless numbers is an academic one; on the one hand it makes the results more generally applicable but on the other hand; it is not appealing to designers, especially due to confusion that arise when everyone uses his own dimensionless numbers. The feed number Λ suggested by the discusser is not applicable here because, his C_d is not a constant and it does not account for transition from orifice to inherent compensation. Further, we would prefer to take the minimum gapheight as a reference instead of h_{out}, incase they are not equal. Instead of the squeeze number σ the transition time of air through the bearing could be used to make frequency dimensionless. It is much more natural for dynamic test purposes to stay with physical units, than characteristic frequencies (like resonances of the measuring setup or 50/60 Hz peak) are easily recognized. Also we are not performing a parametric study of bearings here.

3. For us the use of FEM is obvious, first, because we use a standard package that is completely open for inserting one's own elements and that takes care of administration and matrix solving and second, because FEM can incorporate the restrictor flow boundary condition in a natural way. We can reassure Mr. Al-Bender that we did compare our dynamic calculation results with Dr. Plessers in the past and that these results are in perfect agreement. We both had no good model for the inlet restrictor flow at that time so we agreed upon equal gap inlet pressures.

4. It is certainly not true that the accuracy of linearization depends on the calculation method. It does depend on the nonlinearity of the load characteristic at the working point. For our applications of these bearings their low level vibration behavior are of interest. We did gauge our measurements by checking the coherence regularly.

5. Regarding the incorporation of a restrictor flow model in the analysis we can appreciate the rewarding remark, in fact we think one must have a reliable model for that flow to be able to predict the bearing behavior in advance. It is also true that we did not include any further time dependence in the flow model but our measurements show good agreement with the calculations so there is no need to further complicate the analysis in the frequency range that we investigated. The Blondeel terms "passive stiffness," "gap transfer function" and "restrictor transfer function" are not directly applicable to our approach, we separate the air film properties from the structure properties, like Plessers did.

6. The next paragraph has remarks that do not make much sense to us. Evidently we failed to prove that we already took care of all the improvements that he has suggested. We do not compensate for errors, even a mass compensation is not needed up to 2500 Hz whereas in the Leuven design a big mass is located in between the bearing and the force transducer that does need compensation. Our accelerometer is used to accurately measure bearing motion at high frequency. The lumped model in our Section 5 was intended to explain why we arrived at such a simple and easy to operate apparatus.

7. We assured the apparatus to be an axial series of masses and springs by minimizing tilting motions. The air bearings in the load generator are mainly responsible for that. The big support structure in Fig. 4 could be misleading but note that it is only connected to the main device by a tiny string and only adds useful mass to the base. Furthermore our preload of the bearing is almost without inertia so we experienced no problems there, and we did not report on "verifying" the system through a test object.

8. We did investigate the tilting motion and now we believe that our adjustment procedure assures good parallel surfaces and that the friction in the ball pivot is working in our advantage. We proved this by measuring under several orientations of the ram. The location of the pivot point above the bearing is a a disadvantage, but it is worse to locate it underneath the bearing because of its weakness. We took only two LVDT's because with central loads the average of the two gives the central displacement and we can see whether a significant tilt exists.

9. The use of LVDT's is not as bad as it seems. They are simple, easy to use and have a large linear range. So there is no need to calibrate for each bearing adjustment. There was no need to improve on their contact phenomena, by fixing the stylus to the moving surface and incorporating an airbearing guide. We do agree that we were surprised by being able to measure up to 450 Hz.

10. The repeatability of the apparatus is very good. The measurements were repeated by another person after a complete reassembly and they agreed very well indeed. The noisy character of the signals in our Fig. 9 in fact proves that we are honest enough not to use a filter to suggest accuracy. Also, we used a small scale, which in particular makes the phase look worse than it is.

11. As one can sense from our reply we feel no need to redesign our apparatus. The agreement with theory is far better than in Plessers and Snoeys (1988), especially at high frequencies where our phase goes to zero and their imaginary part of the stiffness does not.

We still believe we made important progress, both theoretically and experimentally. Theoretically because we incorporated the restrictor flow in the analysis. Experimentally because we developed a simple, easy to use test apparatus that can be used up to higher frequencies for objects with higher stiffnesses. The good agreement between calculation and measurement supports that statement.